

Thruster-Specific Force Estimation and Trending of Cassini Hydrazine Thrusters at Saturn

Joan Stupik* and Thomas A. Burk†

Jet Propulsion Laboratory, California Institute of Technology

The Cassini spacecraft has been in orbit around Saturn since 2004 and has since been approved for both a first and second extended mission. As hardware reaches and exceeds its documented life expectancy, it becomes vital to closely monitor hardware performance. The performance of the 1-N hydrazine attitude control thrusters is especially important to study, because the spacecraft is currently operating on the back-up thruster branch. Early identification of hardware degradation allows more time to develop mitigation strategies. There is no direct measure of an individual thruster's thrust magnitude, but these values can be estimated by post-processing spacecraft telemetry. This paper develops an algorithm to calculate the individual thrust magnitudes using Euler's equation. The algorithm correctly shows the known degradation in the first thruster branch, validating the approach. Results for the current thruster branch show nominal performance as of August, 2015.

Nomenclature

AACS	Attitude and Articulation Control Subsystem
RWA	Reaction Wheel Assembly
RCS	Reaction Control System
OTM	Orbit Trim Maneuver
$I_{s/c}$	Spacecraft inertia matrix, kg-m ²
$\vec{\omega}$	Spacecraft body rate, rad/s
\vec{H}	Angular momentum, Nms
$\vec{\tau}$	Torque, Nm
B_C^W	Direction cosine matrix from RWA frame to spacecraft body frame
J	RWA inertia matrix, kg-m ²
$\vec{\Omega}$	RWA rate, rad/s
\vec{p}	Position relative to mechanical frame, m
\vec{u}	Unit vector
F	Thrust magnitude, N
\vec{r}	Position relative to center of mass, m
N	Number of pulses
δ	Thruster on-time, s
t_r	Rise time, s
t_t	Tail-off time, s
s	Modified on-time, s
Q	Derived matrix combining moment arms and on-time, m-s
<i>Superscript</i>	
B	spacecraft body frame
W	RWA frame

*Guidance and Control Engineer, Guidance and Control Section, Mail Stop 230-104, 4800 Oak Grove Drive, Pasadena, CA 91109-8099.

†Cassini Attitude Control Product Delivery Manager, Guidance and Control Section, Mail Stop 230-104, 4800 Oak Grove Drive, Pasadena, CA 91109-8099.

I. Introduction

Cassini is one of the largest and most complex interplanetary spacecraft that has been constructed and launched. After successfully entering orbit at Saturn in 2004, Cassini fulfilled the prime mission objectives (between 2004 and 2008) and was subsequently approved for first and second extended missions. The mission will end in September of 2017 by safely disposing of the spacecraft in Saturn’s atmosphere. To meet the science objectives, Cassini carries a payload of twelve instruments, including antennae, cameras, and spectrometers. The bulk of these instruments are fixed with respect to the spacecraft body and lack the ability to articulate.¹ Therefore, the Attitude and Articulation Control Subsystem (AACS) must slew the whole spacecraft to point an instrument to a science-specified attitude. As the second extended mission advances and hardware approaches or exceeds life expectancy, it becomes increasingly important to monitor the health of the AACS hardware.

Cassini is a three-axis stabilized spacecraft and achieves attitude control during science observations using either the reaction wheel assembly (RWA) or the reaction control system (RCS) thrusters.² The reaction wheel assembly consists of three active wheels, oriented in a mutually orthogonal configuration centered on the spacecraft body Z-axis (i.e. equidistant from the Z-axis). In addition, there is a spare, fourth wheel that may be articulated to match the positions and replace any of the other three, in case of poor performance or failure. In 2003, this fourth wheel was made active to replace one that was not performing optimally.²

The reaction control system consists of two independent, fully redundant branches of eight thrusters (total of sixteen). These branches are called A-branch and B-branch. On each branch, there are four thrusters oriented along the spacecraft body Z-axis (providing control in the X- and Y-axes) and four along the Y-axis (providing control in the Z-axis). Fig. 1 shows, for one branch, the directions of the thrust vectors applied to the spacecraft by each thruster. Fig. 2 shows the location of the thruster branches relative to the rest of the spacecraft. The thrusters mounted in the Y-axis direction (called the Y-thrusters) fire in opposing couples Y1/Y3 and Y2/Y4. This means, for example, that Y1 and Y3 always fire simultaneously and nominally produce no net ΔV . The thrusters mounted in the Z-axis direction (called the Z-thrusters) fire in non-opposing pairs, with the pair determined by the required torque and a resulting non-zero net ΔV . For example, to produce positive torque about the spacecraft Y-axis, Z1 and Z4 would fire.

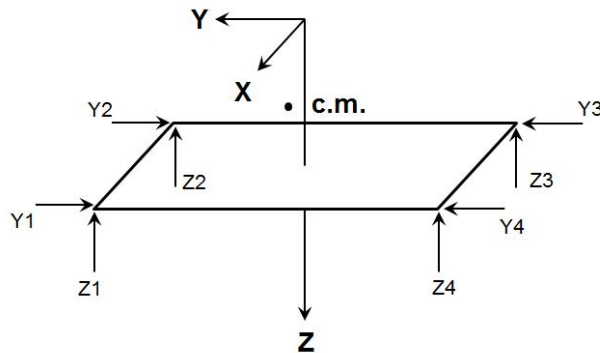


Figure 1. Representative RCS Thruster Branch

The mission began with A-branch as the prime (or active) branch. In 2009, significant degradation in thrusters Z3A and Z4A (see Fig. 1) necessitated a switch to B-branch as the active branch.⁶ This degradation was noted following the navigation team’s radiometric reconstruction of a RCS ΔV maneuver in October of 2008. RCS ΔV maneuvers achieve the desired orbit trim adjustment by firing the four Z-facing thrusters for a fixed cumulative on-time. The October 2008 maneuver resulted in a ΔV about 3% less than expected. Further analysis of RCS propulsion telemetry confirmed the low performance. The underperformance of the thrusters led to a 5.7 m/s penalty spread over subsequent maneuvers to achieve the desired trajectory. Along with the switch to the B-branch thrusters, this paper describes a new tool that was developed to analyze telemetry so that an “early warning” of thruster degradation could be detected more quickly. This tool may help prevent a performance penalty (like the one that resulted from the October 2008 maneuver) in the future.

The reaction wheels achieve more precise pointing than the RCS thrusters and are therefore used during

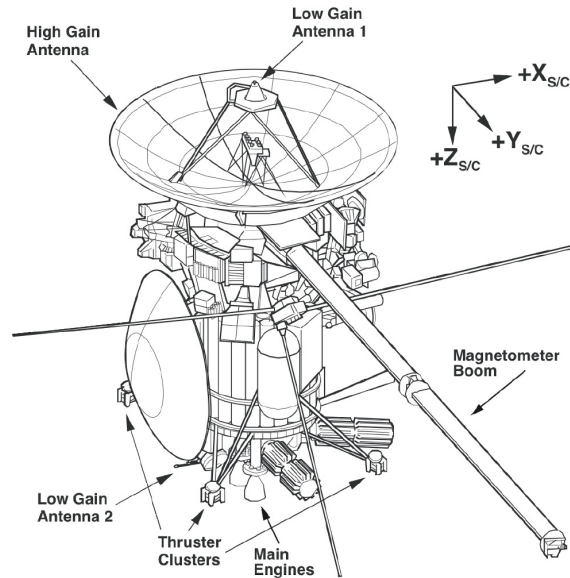


Figure 2. Cassini Spacecraft Diagram

the majority of science observations.³ However, there is a limit to the momentum that may be stored in the wheels. Also, the great variety of science observations requires many different spacecraft orientations. For any given initial reaction wheel momentum setting, a long sequence of orientations almost always results in at least one of the reaction wheels “dwelling” at a very low momentum for many minutes or hours. This can cause reaction wheel bearing degradation (metal-to-metal contact) and eventually lead to the failure of a wheel.⁴ This necessitates the periodic use of the RCS thrusters (approximately five times per orbit⁵) to redistribute the momentum across the wheels in a process called momentum biasing, also known as momentum dumping. Besides momentum biasing, the RCS thrusters are used for a number of other spacecraft activities such as high rate slews, small OTMs, and when encountering large external torques such as low-altitude Titan flybys. In the case of two wheel failures, the mission could feasibly be completed (albeit with less accurate pointing) by using only thrusters for attitude control. However, should multiple thrusters fail, the spacecraft cannot fly solely in the RWA control mode indefinitely due to the required use of thrusters during momentum biasing. A “mixed” branch configuration, in which a subset of thrusters from both A and B branch are prime, has been developed as a contingency for the case in which B-branch begins to show signs of degradation.⁹ This contingency configuration is only valid if there is a functioning thruster from either branch at each of the positions shown in Fig. 1. This means that the mixed branch configuration would not be valid if Z3B or Z4B (on B-branch) degraded, because the corresponding thrusters on A-branch are also unusable.

It is critical to monitor the performance of the B-branch thrusters for signs of degradation. If any thrusters except Z3B or Z4B show signs of reduced performance, early detection would mean a switch to the mixed branch configuration and would nominally prevent a propellant penalty similar to the one resulting from the A-branch degradation. If Z3B or Z4B begin to perform anomalously, early detection will give the operations team more time to develop an action plan. Thruster-specific force trending may be a crucial way to detect such degradation in B-branch thrusters earlier than was possible with the A-branch thrusters.

The thrust of each individual thruster cannot be measured directly. To monitor the performance of individual thrusters, indirect methods must be employed through post-processing of telemetry. This has been a topic of interest to the Cassini spacecraft operations team for many years and there have been some previous publications on the subject. Ref. 7 describes an analytical approach similar to that which will be used in this paper (with a few notable differences) and demonstrates the calculation on a small number of examples. It utilized the Euler equation by balancing reaction wheel spin data with the corresponding thruster firings countering the reaction torque. Ref. 8 applies the approach from Ref. 7 to several years of Cassini data, with some simplifying assumptions and significant filtering.

The purpose of this paper is to improve upon the approach from Ref. 7 and apply the algorithm to many years of Cassini data, using minimal filtering and a different solution method than in Ref. 8. The new solution method provides a more consistent trend of thruster performance and therefore a more reliable insight into the health of the reaction control system. The paper will first outline the analytical method used to calculate the thrust from flight data, listing and justifying simplifying assumptions. It will then discuss the types of thruster events for which the algorithm can provide a reliable thrust estimate. Thrust estimates for approximately the last two years of A-branch are shown and the degradation pattern identified. The thrust for B-branch is then calculated and the trends are discussed.

II. Method

A. Analytic Approach

The indirect method of calculating the individual thruster pulses relies on Euler's rigid body dynamics equation given below.

$$I_{s/c}\dot{\vec{\omega}} + \vec{H}_{RWA} + \vec{\omega} \times (I_{s/c}\vec{\omega} + \vec{H}_{RWA}) = \vec{\tau}_{net} \quad (1)$$

In Eq. (1), $I_{s/c}$ is the spacecraft inertia matrix, $\vec{\omega}$ refers to the spacecraft body rate vector, \vec{H}_{RWA} is the vector containing the momentum from the reaction wheels, $\vec{\tau}_{net}$ is the net external torque, and a dot (e.g. $\dot{\vec{\omega}}$) refers to the time rate of change. All terms in Eq. (1) are in the spacecraft body frame. The following equation converts the reaction wheel rates to momentum in the body frame

$${}^B\vec{H}_{RWA} = {}^B C^W \cdot {}^W J \cdot {}^W \vec{\Omega} \quad (2)$$

where ${}^B C^W$ is the direction cosine matrix to convert a vector in the reaction wheel frame to one in the spacecraft body frame, ${}^W J$ denotes the inertia matrix of the reaction wheels, and ${}^W \vec{\Omega}$ represents a vector containing the reaction wheel rates in radians per second.

It is assumed for this analysis that the only significant external torque is applied by the thrusters. Other external torque sources (gravitational, atmospheric, solar, etc.) are assumed negligible - a reasonable assumption provided that any thruster events taking place close to Titan are disregarded. Integrating Eq. (1) from t_1 to t_2 yields

$$I_{s/c}\Delta\vec{\omega} + \Delta\vec{H}_{RWA} + \int_{t_1}^{t_2} \vec{\omega} \times (I_{s/c}\vec{\omega} + \vec{H}_{RWA})dt = \int_{t_1}^{t_2} \vec{\tau}_{net}dt \quad (3)$$

where Δ indicates the difference between a variable evaluated at t_1 and t_2 . The torque applied to the spacecraft by each individual thruster, i , is the cross product of the thruster position (relative to the center of mass) with the thrust vector. The total torque applied to the spacecraft is the sum of the torque provided by each thruster.

$$\vec{\tau}_{net} = \sum_{i=0}^8 \vec{\tau}_i = \sum_{i=0}^8 \{(\vec{p}_{i,thruster} - \vec{p}_{CM}) \times \vec{u}_i F_i\} \quad (4)$$

where $\vec{p}_{i,thruster}$ is the position of thruster i with respect to the spacecraft mechanical frame, \vec{p}_{CM} is the position of the center of mass with respect to the spacecraft mechanical frame, \vec{u}_i is the unit direction vector of thruster i , and F_i is the thrust magnitude. If the mechanical misalignment of the thrusters is assumed negligible (i.e. Z-thrusters are mounted exactly along the spacecraft Z-axis), the unit direction vectors can be constructed from Fig. 1.

Assuming no change in the center of mass over a small thruster event, all terms in Eq. (4) are constant in the spacecraft mechanical frame with the exception of the thrust magnitude. Hence, Eq. (3) and Eq. (4) can be combined, while letting \vec{r}_i represent the position relative to the center of mass ($\vec{p}_{i,thruster} - \vec{p}_{CM}$) and $\Delta\vec{H}$ denote the total change in angular momentum in the spacecraft mechanical frame [$I_{s/c}\Delta\vec{\omega} + \Delta\vec{H}_{RWA} + \int_{t_1}^{t_2} \vec{\omega} \times (I_{s/c}\vec{\omega} + \vec{H}_{RWA})dt$], into

$$\Delta\vec{H} = \sum_{i=0}^8 \{\vec{r}_i \times \vec{u}_i \int_{t_1}^{t_2} F_i dt\} \quad (5)$$

In an ideal case, the thrust magnitude would be constant (modeled as the red line in Fig. 3). In reality, it takes time for the thruster to reach full thrust after the valve is opened (called “rise” time) and some time to decay after valve is closed and the fuel liquid and vapor in the line and injection chamber disperse (called “tail-off” time). For long thruster on-times, these contributions are negligible. However, many of the events for which the algorithm will be used (i.e. biasing events) operate the thrusters in short 0.125 second pulses. Accurately modeling the thruster pulses improves the thrust estimate.

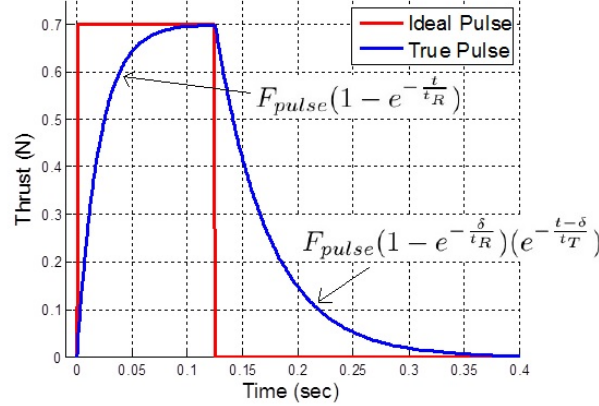


Figure 3. Ideal and True Pulse Models

Both an ideal model and a true model are shown for a representative pulse in Fig. 3. As shown, the rise and tail-off times are modeled with exponential functions. The thrust is denoted by F_{pulse} , δ represents the on-time of the pulse (0.125 seconds), while t_R and t_T represent the rise and tail-off times, respectively.

The integral from t_1 to t_2 of the thrust magnitude in Eq. (5) can be expressed as the product of the number of pulses (N_i) on thruster i in that time span and the integral over one pulse. Using the pulse model expressions in Fig. 3, this integral can be expressed as

$$\int_{t_1}^{t_2} F_i dt = N_i \int_{pulse} F_i dt = N_i F_i [\delta + (t_T - t_R)(1 - e^{-\frac{\delta}{t_R}})] = F_i \Delta s_i \quad (6)$$

where Δs_i is the modified total on-time of thruster i from t_1 to t_2 , accounting for the effects of the rise and tail-off times. Let $i = 1, 2, 3, 4, 5, 6, 7, 8$ equal Y1, Y2, Y3, Y4, Z1, Z2, Z3, and Z4, respectively, and let $\vec{r}_i = [r_{i,x} \ r_{i,y} \ r_{i,z}]^T$. Substituting Eq. (6) into Eq. (5), then executing the matrix multiplication and summation (assuming no mechanical misalignment in vectors \vec{u}_i) yields

$$\Delta \vec{H} = \begin{bmatrix} r_{Y1,z} & r_{Y2,z} & -r_{Y3,z} & -r_{Y4,z} & -r_{Z1,y} & -r_{Z2,y} & -r_{Z3,y} & -r_{Z4,y} \\ 0 & 0 & 0 & 0 & r_{Z1,x} & r_{Z2,x} & r_{Z3,x} & r_{Z4,x} \\ -r_{Y1,x} & -r_{Y2,x} & r_{Y3,x} & r_{Y4,x} & 0 & 0 & 0 & 0 \end{bmatrix} \begin{bmatrix} F_{Y1} \Delta s_{Y1} \\ F_{Y2} \Delta s_{Y2} \\ F_{Y3} \Delta s_{Y3} \\ F_{Y4} \Delta s_{Y4} \\ F_{Z1} \Delta s_{Z1} \\ F_{Z2} \Delta s_{Z2} \\ F_{Z3} \Delta s_{Z3} \\ F_{Z4} \Delta s_{Z4} \end{bmatrix} \quad (7)$$

As mentioned in Section I, the Y-thrusters fire in couples Y1/Y3 and Y2/Y4 (i.e. the on-times are exactly equal within each couple). Under the assumption that mechanical misalignments are negligible, only the *combined* torque about the Z-axis from a pair of Y-thrusters can be calculated using the method described here. It is therefore convenient to assume that the thrust magnitudes of Y1 and Y3 are equal, while those of Y2 and Y4 are equivalent. With this assumption and the knowledge that, for Cassini, $r_{Y1,z} = r_{Y2,z} = r_{Y3,z} = r_{Y4,z}$, Eq. (7) can be rewritten as

$$\begin{bmatrix} \Delta H_x \\ \Delta H_y \\ \Delta H_z \end{bmatrix} = \begin{bmatrix} 0 & 0 & -r_{Z1,y} & -r_{Z2,y} & -r_{Z3,y} & -r_{Z4,y} \\ 0 & 0 & r_{Z1,x} & r_{Z2,x} & r_{Z3,x} & r_{Z4,x} \\ r_{Y3,x} - r_{Y1,x} & r_{Y4,x} - r_{Y2,x} & 0 & 0 & 0 & 0 \end{bmatrix} \begin{bmatrix} F_{Y1/3} \Delta s_{Y1/3} \\ F_{Y2/4} \Delta s_{Y2/4} \\ F_{Z1} \Delta s_{Z1} \\ F_{Z2} \Delta s_{Z2} \\ F_{Z3} \Delta s_{Z3} \\ F_{Z4} \Delta s_{Z4} \end{bmatrix} \quad (8)$$

where subscripts Y1/3 and Y2/4 indicate a value common to each thruster couple. In Eq. (8) it is clear that the equations for the y- and z-thrusters are decoupled and can therefore be separated into

$$\Delta H_z = \begin{bmatrix} (r_{Y3,x} - r_{Y1,x}) \Delta s_{Y1/3} & (r_{Y4,x} - r_{Y2,x}) \Delta s_{Y2/4} \end{bmatrix} \begin{bmatrix} F_{Y1/3} \\ F_{Y2/4} \end{bmatrix} \quad (9)$$

$$\begin{bmatrix} \Delta H_x \\ \Delta H_y \end{bmatrix} = \begin{bmatrix} -r_{Z1,y} \Delta s_{Z1} & -r_{Z2,y} \Delta s_{Z2} & -r_{Z3,y} \Delta s_{Z3} & -r_{Z4,y} \Delta s_{Z4} \\ r_{Z1,x} \Delta s_{Z1} & r_{Z2,x} \Delta s_{Z2} & r_{Z3,x} \Delta s_{Z3} & r_{Z4,x} \Delta s_{Z4} \end{bmatrix} \begin{bmatrix} F_{Z1} \\ F_{Z2} \\ F_{Z3} \\ F_{Z4} \end{bmatrix} \quad (10)$$

During an RWA bias, each RWA motor applies sufficient torque to cause the wheel to change its momentum at a fixed, constant rate. In flight, it takes approximately one minute to change the wheel speeds by 100 rpm. Each wheel produces torques about the body axes - the wheels are not aligned with the body axes, however, and therefore the torque produced by each wheel has components in several body axes. The direction cosine matrix is shown in Eq. (11), translating the torque produced by the wheels in the reaction wheel frame to the body frame. Note that RWA4 is redundant and articulating. At launch, RWA4 was aligned with RWA1. In 2003, RWA4 was set to the same alignment as RWA3 to replace it as part of the prime set.

$$\begin{bmatrix} T_{x,body} \\ T_{y,body} \\ T_{z,body} \end{bmatrix} = \begin{bmatrix} 0 & -1/\sqrt{2} & 1/\sqrt{2} \\ \sqrt{2/3} & -1/\sqrt{6} & -1/\sqrt{6} \\ 1/\sqrt{3} & 1/\sqrt{3} & 1/\sqrt{3} \end{bmatrix} \begin{bmatrix} T_{RW A1} \\ T_{RW A2} \\ T_{RW A3} \end{bmatrix} \quad (11)$$

While the reaction wheels rates are changing at a constant rate, so too is the spacecraft angular momentum. During a biasing event, the wheel rates are indeed changing at a constant rate but reach their terminal wheel rates at different times. As each wheel completes its rate change, the momentum distribution among the three wheels changes and therefore the direction of the spacecraft momentum changes almost instantaneously. In other words, the momentum change profile is a piecewise linear function. A biasing event can be described as having three “phases” where the rates of change of the wheels and the momentum are constant. At the end of each phase, one of the reaction wheels reaches a constant rate. See Fig. 4 for an illustration of the bias phases during a bias on January 10, 2010. The figure shows the momentum profile in the spacecraft Y-axis in the first plot and the three reaction wheel rate profiles in the following plots. During Phase 1, all three reaction wheels are changing rates. At the end of Phase 1, RWA1 has reached the desired rate and remains at that rate for the remainder of the bias. Similarly, RWA2 completes at the end of Phase 2.

There are some circumstances where the change in momentum (e.g. the slope of the momentum profile) changes polarity in the spacecraft body frame. The bias in Fig. 4 is one of these occurrences. Between Phase 2 and Phase 3, RWA2 reaches its final speed and subsequently remains constant - almost instantaneously, the slope of the spacecraft Y-axis momentum, the first plot in Fig. 4, changes from positive to negative. This is an important consideration in the thrust magnitude analysis because $\Delta \vec{H}_{total} = \Delta \vec{H}_{Phase1} + \Delta \vec{H}_{Phase2} + \Delta \vec{H}_{Phase3} \neq \vec{H}_{end} - \vec{H}_{start}$. The thruster on-times, however, only increase in one-pulse increments during the biasing event and therefore $\Delta s_{total} = \Delta s_{Phase1} + \Delta s_{Phase2} + \Delta s_{Phase3} = s_{end} - s_{start}$.

There are limited scenarios in which this “momentum reversal” can happen. Knowing the reaction wheel configuration in Eq. (11), it can be shown that the reversal can only occur in the spacecraft body Y-axis between Phase 2 and 3. One way to ensure that all of the momentum change in an event is captured is to not include a bias with momentum reversal in the trending analysis. The other option, employed in this

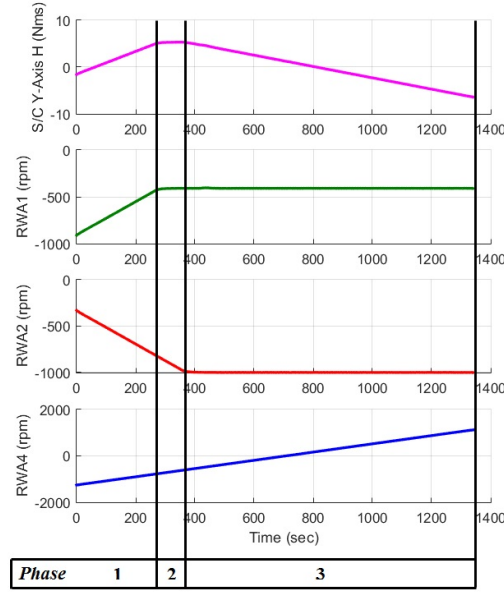


Figure 4. Phases of a RWA Momentum (H) Bias

work, is to disregard Phase 3 when applying Eqs. (9) and (10). Provided that there is sufficient thruster on-time, this option still produces a good thrust estimate.

Eqs. (9) and (10), with momentum change summed over the applicable phases, comprise an underdetermined system of three equations (momentum in each of the three spacecraft body axes) with six unknowns (thruster magnitudes for each y-thruster couple and each of the four z-thrusters). One possible way to create a solvable system is to write a set of three equations at each time interval t_i during the event and assume that the thrust remains the same during the event. This incremental approach creates a system that can sometimes be solved using least squares and a “pseudoinverse”.^{7,8} In many cases, however, the resulting system is linearly dependent and therefore does not result in a reliable solution.

A more robust approach creates a fully determined system of six linearly independent equations by considering the whole momentum change in two distinct thruster events that are close in time. The thrust magnitude will change very little between near-consecutive events, assuming there are no major changes to the center of mass location or moment of inertia between events. Events on Cassini that caused a large, nearly instantaneous change in center of mass or moment of inertia were large ΔV burns (i.e. Saturn Orbit Insertion, SOI), boom deployment, and probe release. The time period addressed in this thrust study begins after the last of these major events.

Let Q_z represent the 1x2 moment arm/on-time matrix in Eq. (9) and Q_{xy} represent the similar 2x4 matrix in Eq. (10). The final, fully determined systems are below

$$\begin{bmatrix} (\Delta H_{total,z})|_{\alpha} \\ (\Delta H_{total,z})|_{\beta} \end{bmatrix} = \begin{bmatrix} (Q_{z,(1x2)})|_{\alpha} \\ (Q_{z,(1x2)})|_{\beta} \end{bmatrix} \begin{bmatrix} F_{Y1/3} \\ F_{Y2/4} \end{bmatrix} \quad (12)$$

$$\begin{bmatrix} (\Delta H_{total,x})|_{\alpha} \\ (\Delta H_{total,y})|_{\alpha} \\ (\Delta H_{total,x})|_{\beta} \\ (\Delta H_{total,y})|_{\beta} \end{bmatrix} = \begin{bmatrix} (Q_{xy,(2x4)})|_{\alpha} \\ (Q_{xy,(2x4)})|_{\beta} \end{bmatrix} \begin{bmatrix} F_{Z1} \\ F_{Z2} \\ F_{Z3} \\ F_{Z4} \end{bmatrix} \quad (13)$$

where $(...)|_{\alpha}$ and $(...)|_{\beta}$ refer to events α and β that occur close enough in time that the thrust magnitude may be assumed to be equivalent and $\Delta H_{total,i}$ represents the total momentum change summed across the three (or two) phases. In theory, α and β would be subsequent events. In practice, however, an event requires a minimum amount of on-time to provide a reasonable estimate. Therefore, some events with very small momentum changes were disregarded in the application of the algorithm.

B. One Pair Y-Thrusters Case

When B-branch became the prime branch after two of the A-branch Z-thrusters degraded, an effort was made to prevent or delay a similar problem on B-branch. The concrete cause of the degradation remains unknown. It was observed, however, that A-branch Z-thrusters had accumulated significantly more throughput than the Y-thrusters. A new method of biasing the reaction wheels, called “Y-biasing”, was developed to attempt a more even distribution of throughput between the Y- and Z-thrusters, in the event that the degradation was related to throughput. A Y-bias involves a turn to align the desired momentum change vector with the spacecraft Z-axis.¹⁰ In cases where these two vectors are perfectly aligned, none of the Z-thrusters would fire and only one Y-thruster pair would fire. There are some situations where a Y-bias is not possible, but throughput on the Z-thrusters has accumulated slower on B-branch than it did on A-branch.

For the Y-bias events, or any event where the on-time is primarily on just one Y-thruster pair (i.e. for one of the Y-thruster pairs, $\Delta s_{Y,pair} \approx 0$), Eq. (9) reduces to one equation (ΔH_Z) and one unknown ($F_{Y1/3}$ or $F_{Y2/4}$). For these cases, an estimate for the thrust magnitude can be obtained independently for each individual event. This “Y-bias” method produces thrust estimates that agree with those from a calculation using Eq. (12) for the same event.

III. Results

The algorithm described above has been applied to a total of approximately seven years of Cassini telemetry. Each thruster event during that time was paired with a nearby event - in some cases, the event immediately prior to the present one. Often, however, the previous thruster event was not deemed suitable for calculating a thrust estimate. Very small momentum changes (i.e. very few thruster firings) are subtle enough that the noise in the telemetry channels dominates the calculation. Through trial and error, a minimum on-time of five seconds was selected. In order for a thruster event to be eligible for calculations, at least two of the Z-thrusters must have more than five seconds of on-time.

First, estimates over the last two years of flying on A-branch (2007-2009) were calculated to verify that the known degradation is identifiable using this method. Results are shown on the left in Fig. 5.

In these plots, the solid (red) line shows the expected thrust, calculated as a function of measured tank pressure. The hydrazine thruster branches are blow-down systems and therefore are expected to experience a decrease in tank pressure over time as hydrazine is consumed. Thrust is approximately linearly proportional to the tank pressure, so a similar thrust reduction over time is expected. The dash-dot (black) lines show $\pm 5\%$ of the expected thrust. This is a reasonable range in which the thrust can be expected to vary from event to event. The solid (black) vertical line denotes the time of the OTM that failed to achieve the desired velocity change and therefore alerted the operations team to the unexpected degradation in the thrusters. Each individual thrusting event is represented with an asterisk (blue). Despite some scatter in the data, trends are visible. The A-branch’s Z1 and Z2 thrusters degraded at a rate consistent with the reduction in tank pressure. By the time the switch to B-branch occurred in early 2009, it is clear from Fig. 5 that Z3A showed degraded performance. In early 2009, degradation is also visible in Z4A, though not as pronounced as in Z3A. Independent assessments made by other subsystems also show significant degradation in Z3A and less (but still notable) degradation in Z4A. At the time of the anomalous OTM in October of 2008, represented in Fig. 5 as a solid vertical line, Z3A has less pronounced but still visible degradation. With this knowledge, the operations team would have noted a problem and possibly could have prevented some of the penalty from the under-performed OTM. At the time of that OTM, Z4A does not have an obvious downward trend - it appears to have just begun to deviate from the expected thrust. Had this tool been monitoring thruster performance during 2008, Z3A would have been flagged with poor performance before the missed OTM. Z4A degradation may not have been identified solely from Fig. 5. However, this analysis could have flagged Z4A as a potential problem if it was coupled with independent estimates from other subsystems - although it is unlikely that preventative action would have been taken based on the trend shown by Z4A in October of 2008.

After verifying that the known thruster degradation in A-branch was apparent using this method of trending the thrust magnitude estimates, similar plots were made for the B-branch Z-thrusters. The right of Fig. 5 contains the plots showing the Z-thruster estimates for all eligible events from the start of B-branch in March of 2009 through July of 2015.

There is less scatter in the Z-thruster data for B-branch than in A-branch. There are also fewer data points for the Z-thrusters after May of 2010, when the operations team began using Y-biases (see Section IIB).

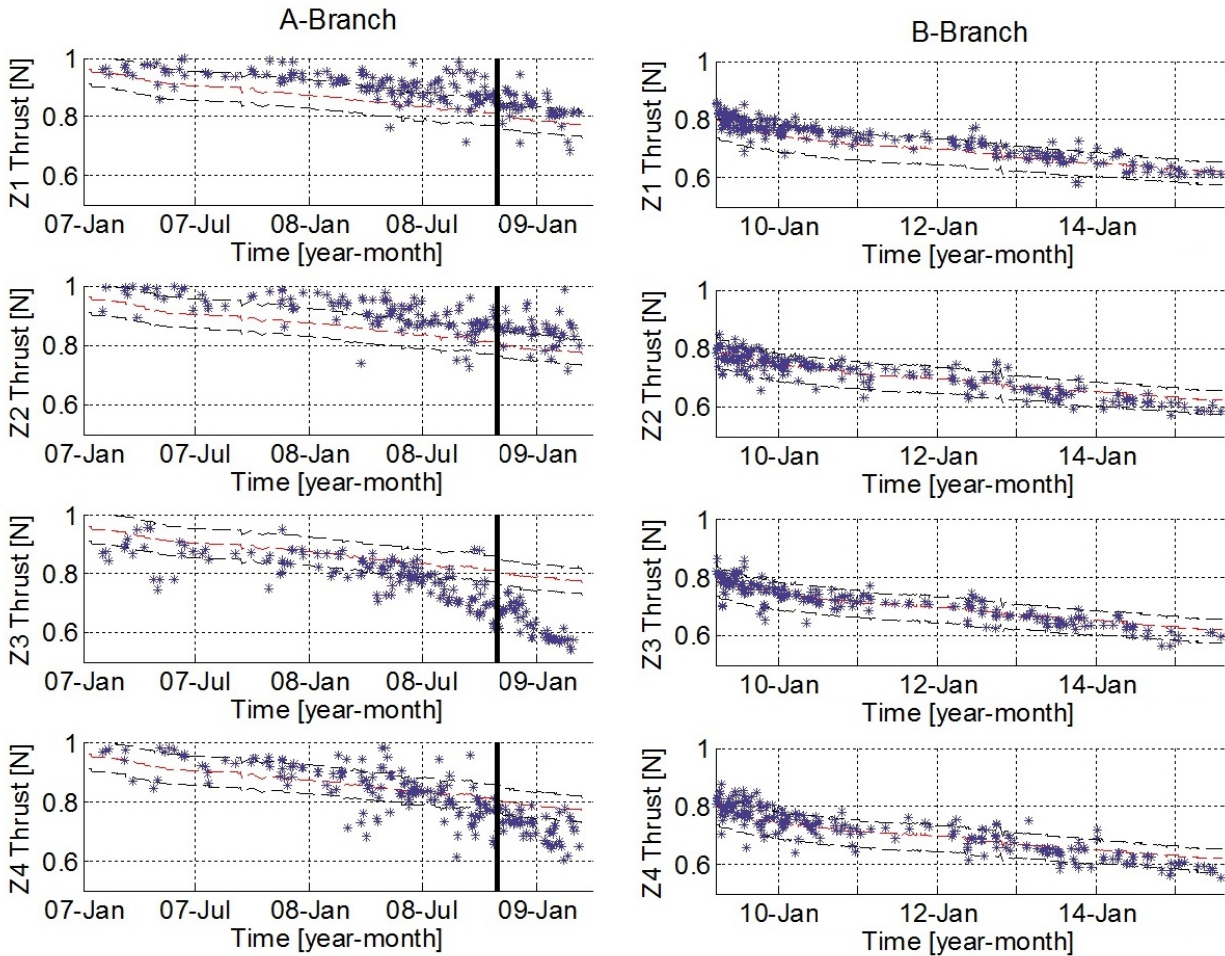


Figure 5. A-Branch (left) and B-Branch (right) Z-Thrusters Thrust Magnitude Estimates. Minimum on-time of 5 seconds. Solid (red) line shows expected thrust. Dash-dot (black) lines show $\pm 5\%$, an envelope of expected deviation. Asterisk (blue) points are thrust estimates. Solid (black) vertical line indicates the time of the OTM in October of 2008 that alerted the team to the thrust degradation.

These Y-biases are designed to use only the Y-thrusters - in practice, there can be a few Z-thruster firings, but no more than a handful of pulses.¹⁰ Due to the small on-times, the Z-thruster estimates from Y-biases are unreliable and therefore are not included in the trending analysis in Fig. 5. Most of the thrust estimates fall within the $\pm 5\%$ envelope of expected deviation from the predicted thrust. As of August 2015, there does not seem to be a worrisome trend for any of the four Z-thrusters. In general, the thrust magnitudes for Z2B and Z4B were slightly above the predicted thrust in 2010 and have drifted slightly below the predicted value in recent years. However, an examination of the degradation in Z3A in Fig. 5 reveals that there is a notable change in slope when the unexpected degradation began. The slow drift in the thrust magnitudes that is observable in Fig. 5 for Z2B and Z4B is not currently cause for alarm.

The Y-thrusters are also monitored - estimates for both branches are shown in Fig. 6. Circles (black) represent the Y1/Y3 pair while the crosses (blue) show the Y2/Y4 pair. The A-branch estimates fall consistently below the expected envelope of deviation, but follow the expected rate of degradation (due to tank pressure) closely. The reason that the estimates fall consistently under the predicted thrust is unknown. One possible contributor is a misrepresentation of the rise and tail times. The thrust estimates are sensitive to these parameters. The rise time is assumed constant throughout the mission while the tail-off time has been updated a total of four times. A discrepancy between the true rise or tail times and those used by ground software would appear as a constant offset. Despite this offset, it can be observed that there is no indication of the Z3A sharp slope change signature. The B-branch estimates virtually all fall within -5% to

0% of the predicted thrust and also closely follow the expected rate of degradation. There is no worrisome trend apparent in either the A-branch or B-branch Y-thrusters.

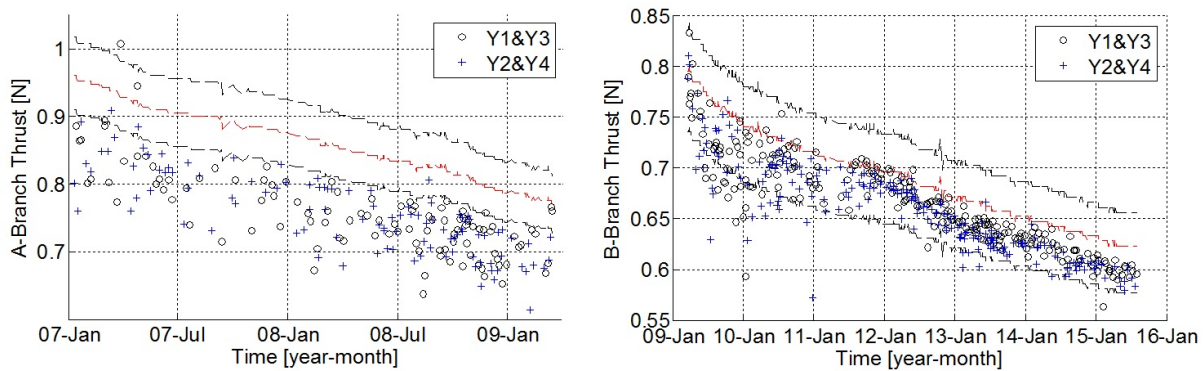


Figure 6. A-Branch (left) and B-Branch (right) Y-Thruster Pairs Thrust Magnitude Estimates. Minimum on-time of 5 seconds. Solid (red) line shows expected thrust. Dash-dot (black) lines show $\pm 5\%$, an envelope of expected deviation. Circles (black) indicate estimates for the Y1/Y3 pair while crosses (blue) represent the Y2/Y4 pair.

The estimates in Fig. 6 are calculated using the method described in Section IIB, the one-event calculation. When the on-time of one thruster pair is negligible, the problem reduces to one equation and one unknown. A unique estimate can be obtained for just one event - there is no need to pair the event with a previous one to get a fully-determined system. An estimate from two events can still be calculated, but there is not a significant difference between the two calculated values. Fig. 7 shows the two calculations plotted together.

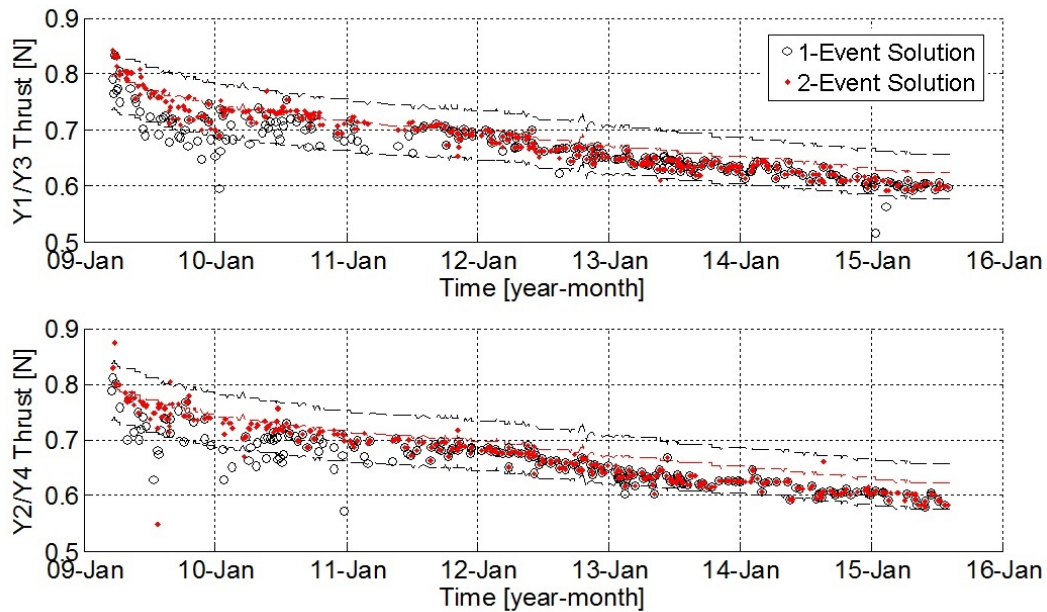


Figure 7. Y1/Y3 (top) and Y2/Y4 (right) Y-Thrusters Pair Thrust Magnitude Estimates. Minimum on-time of 5 seconds. Solid (red) line shows expected thrust. Dash-dot (black) lines show $\pm 5\%$, an envelope of expected deviation. Circles (black) represent one-event estimates while diamonds (red) denote two-event estimates.

IV. Conclusion

The Cassini spacecraft launched in 1997 and arrived at Saturn in 2004, where it has been studying Saturn, the rings, and the moons. The project is currently in its second extended mission and is scheduled to continue until September of 2017. It is crucial to carefully monitor hardware as it reaches and exceeds the documented lifetimes. Early indications of degradation in critical flight hardware provide more time in which to develop mitigation strategies. The 1-N attitude control thrusters are members of this critical hardware, especially because the spacecraft has been operating on the back-up thruster branch since 2009. The degradation in the A-branch was not detected until a burn failed to achieve the desired ΔV , resulting in a propellant penalty of several kilograms. In the second extended mission, there is little remaining propellant. The algorithm described in this work is one tool to monitor thruster performance. It uses Euler's equation to calculate an individual estimate of thrust magnitude for each thruster, using telemetry from the spacecraft (i.e. body rates, reaction wheel rates, and thruster on-time). Despite some scatter in the thrust estimates, the algorithm succeeds in its purpose to detect trends in the thrust magnitudes. The purpose is not to provide an exact thrust magnitude - the noise present in the telemetry prevents it - but to identify signs of unexpected degradation in performance. The algorithm clearly shows the known degradation in the A-branch Z-thrusters. As of the beginning of August, 2015, both the Y- and Z-thrusters show no signs of the type of degradation experienced by the A-branch thrusters. This method, when coupled with other independent detection methods, will continually monitor the thruster health and identify any performance problems early enough to allow for mitigation strategies to be explored.

Acknowledgments

The work described in this work was carried out at the Jet Propulsion Laboratory, California Institute of Technology, under contract with the National Aeronautics and Space Administration. Reference to any specific commercial product, process, or service by trade name, trademark, manufacturer, or otherwise, does not constitute or imply its endorsement by the United States Government or the Jet Propulsion Laboratory, California Institute of Technology. We wish to acknowledge Samantha Krening, who worked on a preliminary version of this algorithm.

References

- ¹Gibbs, R., "Cassini Spacecraft Design," Proc. SPIE Vol. 2803, p. 246–258, Cassini/Huygens: A Mission to the Saturnian Systems, Linda Horn; Editor.
- ²Lee, Allan Y. and Hanover, Gene, "Cassini Spacecraft Attitude Control System Flight Performance," AIAA-2005-6269, *Proceedings of the AIAA Guidance, Navigation, and Control Conference, and Exhibit*, San Francisco, CA, Aug. 15–18, 2005.
- ³Pilinski, E. and Lee, A. Y., "Pointing Stability Performance of the Cassini Spacecraft," *Journal of Spacecraft and Rockets*, Volume 46, No. 5, September–October, 2009, pp. 1007–1015.
- ⁴Mittelsteadt, C. O., "Cassini Attitude Control Operations - Guidelines Levied on Science to Extend Reaction Wheel Life," AIAA-2011-6553, *Proceedings of the AIAA Guidance, Navigation, and Control Conference, and Exhibit*, Portland, OR, Aug. 8–11, 2011.
- ⁵Luna, Michael E., and Bates, David M., "The Challenge of Implementing RWA Biases on the Cassini Spacecraft during Extended Mission Sequence Development," AIAA 2009-5764, *Proceedings of the AIAA Guidance, Navigation, and Control Conference*, Chicago, IL, August 10–13, 2009.
- ⁶Mizukami, M., Barber, T. J., Christodoulou, L. N., Guernsey, C. S., and Haney, W. A., "Cassini Spacecraft Reaction Control System Thrusters Flight Experience," *JANNAF Propulsion Meeting*, Colorado Springs, Colorado, May 2010.
- ⁷Feldman, A. and Lee, A. Y., "In-Flight Estimations of Cassini Spacecraft Inertia Tensor and Thruster Magnitude," AAS 2006-102, *Proceedings of the AIAA Guidance, Navigation, and Control Conference*, San Diego, CA, Jan. 22–26, 2006.
- ⁸Rizvi, F., Cassini Thruster Calibration Algorithm Using Reaction Wheel Biasing Data, *Journal of Spacecraft and Rockets*, Volume 51, No. 2, March–April, 2014, pp. 563573.
- ⁹Bates, D., Lee, A. Y., Meakin, P., and Weitzl, R., "Fault Protection Design and Testing for the Cassini Spacecraft in a 'Mixed' Thruster Configuration," *Proceedings of the AIAA Guidance, Navigation, and Control Conference*, Boston, MA, Aug. 19–22, 2013.
- ¹⁰Brown, T. S., "Y-Biasing: A New Operational Method for Cassini to Control Thruster Usage while Managing Reaction Wheel Momentum," AIAA 2010-7560, *Proceedings of the AIAA Guidance, Navigation, and Control Conference*, Toronto, Ontario Canada, August 2–5, 2010.